Numerical Solution of the Simple Monge–Ampère Equation with Non-convex Dirichlet Data on Non-convex Domains

Max Jensen

Abstract. The existence of a unique numerical solution of the semi-Lagrangian method for the simple Monge–Ampère equation is known independently of the convexity of the domain or Dirichlet boundary data—when the Monge–Ampère equation is posed as Bellman problem. However, the convergence to the viscosity solution has only been proved on strictly convex domains. In this paper we provide numerical evidence that convergence of numerical solutions is observed more generally without convexity assumptions. We illustrate how in the limit multi-valued functions may be approximated to satisfy the Dirichlet conditions on the boundary as well as local convexity in the interior of the domain.

Keywords. Monge-Ampère equation, Bellman equation, semi-Lagrangian method.

AMS classification. 49L25, 65N99.

1 Introduction

The paper is concerned with the numerical computation of solutions of the so-called simple Monge–Ampère equation

$$\det(D^2u) = \left(\frac{f}{2}\right)^2 \qquad \text{in } \Omega, \tag{1.1a}$$

$$u(x) = g(x) \qquad \text{on } \partial\Omega, \tag{1.1b}$$

where $\Omega \subset \mathbf{R}^2$, $g \in C(\mathbf{R}^2)$ and $f \in C(\Omega)$ is non-negative: $f \geq 0$.

This raises immediately the question how the notion of solution for (1.1) should be defined. Beyond classical solutions, the generalisations in the Aleksandrov and viscosity sense provide settings of less smooth solutions. Any such definition in the literature imposes implicitly or explicitly convexity properties on u.

If Ω is non-convex but it is known that there exists a locally convex subsolution which attains the boundary data pointwise, then the works [7, 8] give criteria for the existence of a unique solution. If Ω is convex (possibly not strictly) and g non-convex then [1] examines in the context of the closely related Gauss curvature problem the possibility of solutions which are in a certain sense multi-valued on $\partial\Omega$. We shall return to these results in sections 3 and 4.

To our knowledge there has been no systematic analysis of the well-posedness of (1.1) for the combination of a non-convex domain and general non-convex boundary data. It is therefore interesting if numerical methods can provide an insight into (1.1) in this case. The basis for our study is [6] where a semi-Lagrangian numerical scheme is proposed, which uses Krylov's Bellman reformulation [13] of (1.1). A closely related numerical scheme is considered in [14]. While the convergence proof to viscosity solutions in [6] requires strict convexity of Ω in order to make a comparison principle available, we highlight two results in that work which do not impose any form of convexity on Ω or g:

(a) For any finite element mesh there exists a unique numerical solution u_i, which is the limit of a globally converging semi-smooth Newton method.

(b) There exists a constant C (depending on Ω, f and g only) such that $\|u_i\|_{L^\infty} \leq C$ for all numerical solutions u_i independently of the mesh.

Thus at this point we know that as the finite element mesh size h approaches 0 some subsequences of numerical solutions converge weakly* to functions in L^∞, which may be candidate solutions of (1.1) of some form.

The aims of this paper are

(a) to provide numerical evidence that indeed not just subsequences but the whole sequence of numerical solutions converges, provided that the stencil size is scaled appropriately with the mesh size;

(b) to highlight that the Bakelman interpretation of solutions might extend to the non-convex setting, consistently with the findings in [7, 8];

(c) to study the performance of the numerical scheme in the non-convex setting, e.g. the robustness of the semi-smooth Newton solver;

(d) to present computations on general domains, e.g. which are not Lipschitz.

2 The Bellman formulation and its semi-Lagrangian approximation

A difficulty when solving (1.1) is that the Monge–Ampère operator $v \mapsto \det(D^2 u)$ is only elliptic on the set of convex functions. It is therefore convenient to reformulate the problem in such a way that the set of solutions remains unchanged but ellipticity is established on the whole function space.

For that purpose we define the Bellman operator

$$H(A, f) := \sup_{B \in \mathbf{S}_1} \left(-B : A + f \sqrt[d]{\det B} \right) \qquad \forall A \in \mathbf{S}, f \in [0, \infty), \tag{2.1}$$

where $\mathbf{S}$ is the set of symmetric 2×2 matrices, $\mathbf{S}_+ := \{A \in \mathbf{S};\, A \geq 0\}$ and $\mathbf{S}_1 := \{B \in \mathbf{S}_+;\, \operatorname{tr} B = 1\}$, and consider the boundary value problem

$$H\big(D^2u(x), f(x)\big) = 0 \qquad \forall x \in \Omega, \tag{2.2a}$$

$$u(x) = g(x) \qquad \forall x \in \partial\Omega. \tag{2.2b}$$

It was shown [6] that

$$\begin{aligned} &\{v \in C(\overline{\Omega}) : v \text{ is convex and a viscosity solution of (1.1a)}\} \\ &= \{v \in C(\overline{\Omega}) : v \text{ is a viscosity solution of (2.2a)}\}. \end{aligned} \tag{2.3}$$

This statement does not require boundedness or convexity of Ω and does in this form not refer to the boundary conditions.

To discretize (2.2a) we write $B = \sum_i \lambda_i\, e_i\, e_i^{\mathsf{T}} \in \mathbf{S}_1$ with the eigenvalues λ_i and normalised eigenvectors e_i, so that for smooth functions ϕ

$$\begin{aligned} B : D^2\phi(x) &= \sum_i \lambda_i (e_i\, e_i^{\mathsf{T}}) : D^2\phi(x) = \sum_i \lambda_i\, \partial^2_{e_i,e_i}\phi(x) \\ &= \sum_i \lambda_i \frac{\phi(x + ke_i) - 2\phi(x) + \phi(x - ke_i)}{k^2} + \mathcal{O}(k^2). \end{aligned}$$

Evaluating these central differences on a P1 finite element space at interior nodes, combined with nodal interpolation of g on $\partial\Omega$, gives the numerical scheme of [6].

Remark 2.1. A comparison principle on the set of semi-continuous functions in respect to H holds when classical boundary conditions are considered [6], where Ω may be non-convex. For the proof of convergence this comparison principle is applied to the upper and lower semi-continuous envelopes of the sequence of numerical solutions—in the setting of strictly convex domains where it is ensured that the envelopes attain the boundary conditions in the classical sense.

The numerical experiments in this paper highlight that on non-convex domains the envelopes may only satisfy the boundary conditions in a generalised form. It would be most convenient if the convergence proof could be translated to viscosity boundary conditions as they are defined either in [2] or alternatively in the form of [4]. However, in [12] counterexamples were given to show that comparison principles with these kinds of viscosity boundary conditions do in general not hold on the spaces of semi-continuous functions (even if Ω is convex), screening out trivial extensions of the proof.

3 The Monge–Ampère equation on non-convex domains

In the light of Remark 2.1, we wish to identify settings in which the exact solution of (1.1) satisfies the boundary conditions classically. It was shown in [7] that this is

guaranteed provided one knows of the existence of a strict subsolution and sufficient smoothness of data and domain. Indeed [7] covers a more general equation with dependence on first-order derivatives.

Theorem 3.1 (Guan and Spruck '93). *Let $\Omega \subset \mathbf{R}^n$ be a smooth bounded domain with boundary components $\partial\Omega = (\gamma_1, \ldots, \gamma_m)$. Assume that there is a smooth, strictly locally convex function $\underline{u}$ in $\overline{\Omega}$ satisfying*

$$\det(\underline{u}_{ij}) \geq \psi(x, \underline{u}, \nabla \underline{u}) + \delta_0 \quad \text{in } \Omega,$$
$$\underline{u} = \phi \quad \text{on } \partial\Omega,$$

where ϕ and ψ are smooth, $\psi > 0$ and $\psi^{1/n}(x, u, p)$ is convex in p. Then there is a smooth locally convex solution $u \in C^\infty(\overline{\Omega})$ to the Monge–Ampère boundary-value problem:

$$\det(u_{ij}) = \psi(x, u, \nabla u) \quad \text{in } \Omega,$$
$$u = \phi \quad \text{on } \partial\Omega.$$

If $\psi_u \geq 0$, then the solution is unique.

A similar result can be found in [8], with vanishing right-hand side but a more precise specification of the required regularity.

Theorem 3.2 (Guan '98). *Assume that $\partial\Omega$ is in $C^{3,1}$ and $\phi \in C^{3,1}(\partial\Omega)$. Suppose there exists a locally strictly convex function $\underline{u} \in C^2(\overline{\Omega})$ with $\underline{u} = \phi$ on $\partial\Omega$. There is a unique locally convex weak solution of*

$$\det(u_{ij}) = 0 \quad \text{in} \quad \Omega, \quad u = \phi \quad \text{on} \quad \partial\Omega$$

in $C^{1,1}(\overline{\Omega})$.

Our first computational experiment concerns the convergence of the numerical approximations to an exact solution, for which we know from the above that the boundary conditions are admitted classically.

Experiment 3.1 (Quartic problem on a ring). We approximate the exact solution $u(x) = g(x) = (x_1^2 + x_2^2)^2$ on the ring:

$$\Omega = \{x \in \mathbb{R}^2 : \|x\|_2 \in (\tfrac{1}{2}, 1)\}.$$

The quasi-uniform grid has at the coarsest level 177 nodes and at the finest level after 6 uniform refinements 563, 712 nodes. The stencil diameter k is, away from the boundary, represented through $k = m \cdot h$ by a fixed positive factor m and the (average) mesh size h. Near the boundary, so where $m \cdot h$ is larger than the distance to $\partial\Omega$, the stencil is reduced in size to remain within Ω, cf. [6].

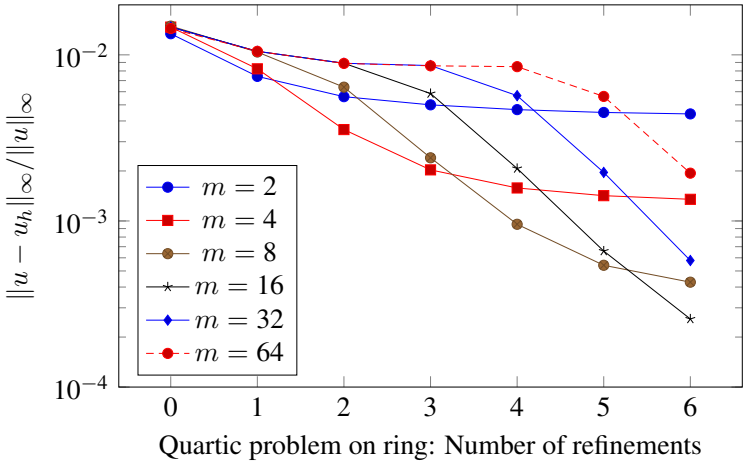

Figure 1. Relative L^∞-error for the test problem of Experiment 3.1.

Figure 1 shows the decay of the relative $L^\infty(\Omega)$ approximation error for different choices of the multiplier $m \in \{2, 4, 8, 16, 32, 64\}$. As predicted by the Wasow-Motzkin theorem [15], $h/m \to 0$ and $m \to \infty$ as $h \to 0$ are necessary to ensure convergence. Similarly it is expected that on fine meshes larger values of m, e.g. $m = \sqrt{h}$, give a smaller error than smaller m, e.g. $m = h$. The table shows the multiplier m which achieves the smallest relative L^∞ error for a given number of degrees of freedom, and the number of Newton iterations of the respective computations to obtain a Newton step size of less than 5e-8 in the ∞-norm:

DoFs	177	628	2352	9088	35712	141568	563712
m	2	2	4	4	8	8	16
rel. L^∞-error	1.3e-2	7.4e-3	3.6e-3	2.0e-3	9.6e-4	5.4e-4	2.6e-4
# Newton	4	5	6	7	7	7	8

Importantly, the table gives numerical evidence of the convergence of the scheme on a non-convex domain without the necessity to pass to a subsequence if m is selected suitably.

In the next experiment the computational domain is less regular than the requirements of Theorems 3.1 and 3.2 demand; however, a subsolution is still known to exist. As before the whole sequences of numerical solutions appear to converge provided that $h/m \to 0$ and $m \to \infty$ as $h \to 0$.

Experiment 3.2 (Quartic problem on L-shape). We approximate the exact solution $u(x) = (x_1^2 + x_2^2)^2$ on the L-shape:

$$\Omega = \big[(0,1) \times (-1,1)\big] \cup \big[(-1,1) \times (0,1)\big].$$

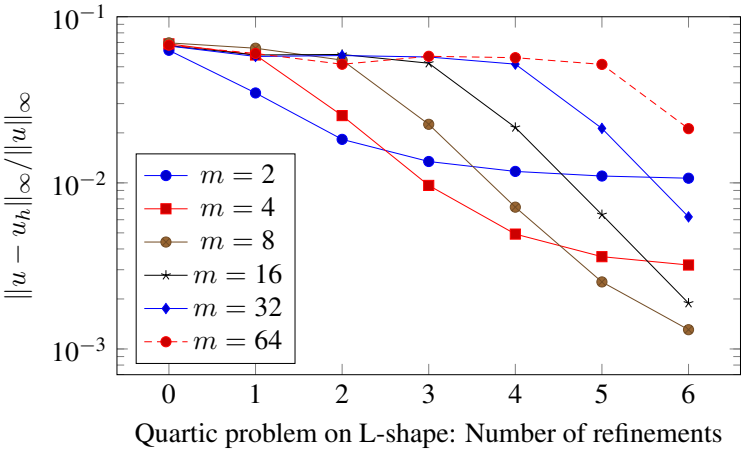

Figure 2. Relative L^∞-error for the test problem of Experiment 3.2.

The grid has at the coarsest level 58 nodes and at the finest level after 6 uniform refinements 168,961 nodes. Figure 2 shows the decay of the relative $L^\infty(\Omega)$ approximation error, while the below table is structured as in the previous experiment. Overall the largest number of Newton iterations in this computational experiment is 9, which occurs on the finest mesh with $m = 32$.

DoFs	58	197	721	2753	10753	42497	168961
m	2	2	2	4	4	8	8
rel. L^∞-error	6.2e-2	3.5e-2	1.8e-2	9.6e-3	4.9e-3	2.5e-03	1.3e-3
# Newton	5	6	5	7	7	8	8

4 The simple Monge–Ampère equation with non-convex boundary data

In computational experiments where the domain Ω is not strictly convex and there is no subsolution $\underline{u}$ as in the above Theorems 3.1 and 3.2 we observe numerical solutions which appear to approximate multi-valued boundary data.

Experiment 4.1 (Non-convex boundary data on convex domain). Now

$$\Omega = B_1(0) \cup \big[(0,1)\times(0,1)\big] = \{x \in \mathbf{R}^2 : \|x\| < 1\} \cup \big[(0,1)\times(0,1)\big]$$

is a convex but not strictly convex domain. On the vertical straight boundary segment $\Gamma := \partial\Omega \cap \big[\{1\}\times(0,1)\big]$ we impose the non-convex boundary data $g(x) = x_2(1-x_2)$ while on the remainder $\partial\Omega \setminus \Gamma$ we set $g(x) = x_1^4 - 1$. We select $f = 0$ on Ω, implying that the graph of the solution u is a surface of vanishing Gauss curvature.

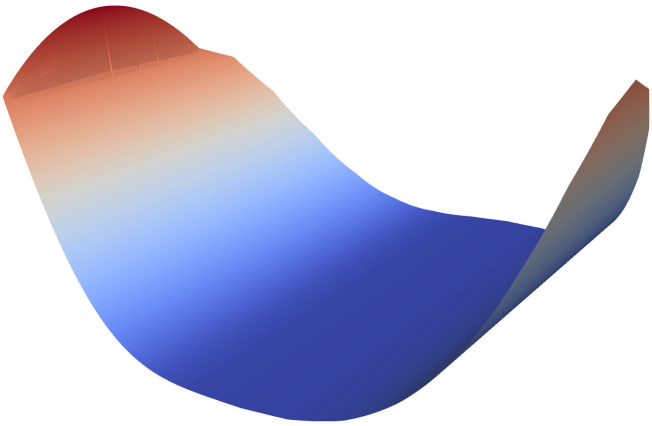

(a)

(b)

Figure 3. Plot (a) shows the numerical solution of Experiment 4.1 on the finest mesh. Notice the approximation to a multi-valued solution on the far side. Here the computational domain is given by the approximation of Ω with the coarsest mesh, which is not changed in the course of the refinement. In (b) we see the difference between the numerical solution and $x_1^4 - 1$, highlighting how localised the effect of the non-convex section of g on the numerical solution is.

A numerical solution is shown in Figure 3. In the vicinity of Γ on the far side of the plot the numerical solution is nearly vertical, interpolating on Γ the data $g(x) = x_2(1-x_2)$ while attaining at the interior nodes neighbouring Γ approximately the value $x_1^4 - 1 \approx 0$.

Recalling from (2.3) that the Bellman formulation enforces convexity on the domain Ω of the differential operator, it appears that the boundary data is only extended into the interior of the domain in as far as convexity permits. Indeed, according Figure 4 the numerical solutions converge on the subdomain $\omega := \{x \in \Omega : x_1 < 0.95\}$ under mesh refinement to $u(x) = x_1^4 - 1$; we see a relative $L^\infty(\omega)$ error of $1.35 \cdot 10^{-4}$ on a mesh with 304129 DoFs and $m = 64$.

The table gives the numerical values of the error for the best choices of m on a given mesh, and the associated number of Newton iterations:

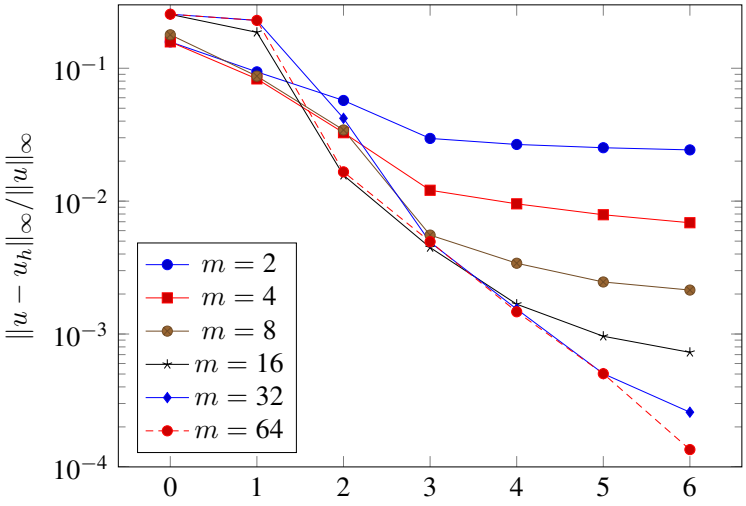

Figure 4. Relative $L^\infty(\omega)$-error for the test problem of Experiment 4.1.

DoFs	145	329	1249	4865	19201	76289	304129
m	2	4	16	16	64	64	64
rel. L^∞-error	1.6e-1	8.3e-2	1.6e-2	4.5e-3	1.5-3	5.0e-04	1.4e-4
# Newton	6	6	9	10	12	14	19

Overall the largest number of Newton iterations in this computational experiment is 19, which occurs on the finest mesh with $m = 64$.

To give an interpretation of Experiment 4.1 we review a result due to Bakelman [1]. Let v be a bounded convex function on Ω and $\overline{Co}(\Gamma_v)$ be the closed convex hull of the graph $\Gamma_v \subset \mathbf{R}^{2+1}$ of v. Then the function

$$\nu_v : \partial\Omega \to \mathbf{R}, \; x \mapsto \inf\{h \in \mathbf{R} : (x, h) \in \overline{Co}(\Gamma_v)\}$$

is called the border of the function v. For fixed given right-hand side f we denote by $\mathcal{L}$ the set of functions v which satisfy the Monge-Ampère differential equation in the Aleksandrov sense and

$$\nu_v(x) \leq g(x) \qquad \forall x \in \partial\Omega.$$

If the domain Ω is strictly convex then Aleksandrov and viscosity solutions coincide for the simple Monge-Ampère equation: See [9] for the proof when the continuous f is positive. This argument can be extended to the case of non-negative f with the tools of [5]—alternatively one can use the uniqueness of solutions and [6].

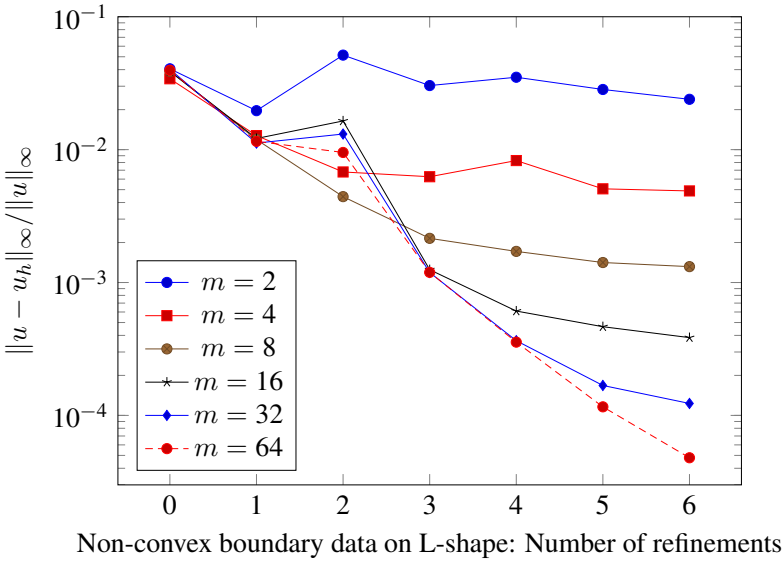

Figure 5. Relative $L^\infty(\omega)$-error for the test problem of Experiment 5.1.

In the context of the Gauss curvature problem, Bakelman shows under a data condition that on bounded strictly convex domains Ω the set $\mathcal{L}$ is non-empty. Moreover, there is a unique $u \in \mathcal{L}$ such that $\nu_u \geq \nu_v$ for all $v \in \mathcal{L}$. This u is considered to be the generalised solution of the boundary value problem.

The numerical solutions of Experiment 4.1 evidently converge to $u(x) = x_1^4 - 1$ in $L^\infty_{\mathrm{loc}}(\Omega)$, so on relatively compact subsets of Ω. In the present setting, the border of u is its trace. As the numerical solution attains the continuum of values between $g(x)$ and $\nu_u(x)$ in the vicinity of any $x \in \partial\Omega$, the visual impression is that of a convergence to a multi-valued limit which attains the interval $[\nu_u(x), g(x)]$ at x. It is therefore appealing to adopt this multi-valued interpretation for the purposes of this text.

Starting from [1], Froese recently studied a wide-stencil method for the Gauss curvature problem with non-classical boundary conditions on convex domains [10]. There, besides the definition with the border function ν_u, also viscosity boundary conditions as in [4] are discussed. Importantly, the connection between Bakelman's work and numerical convergence analysis is made.

5 The simple Monge–Ampère equation on non-convex domains without a classical subsolution

As far as we are aware there is no systematic analysis in the literature which extends [1, 7, 8] to boundary value problems where non-convex boundary data is imposed on

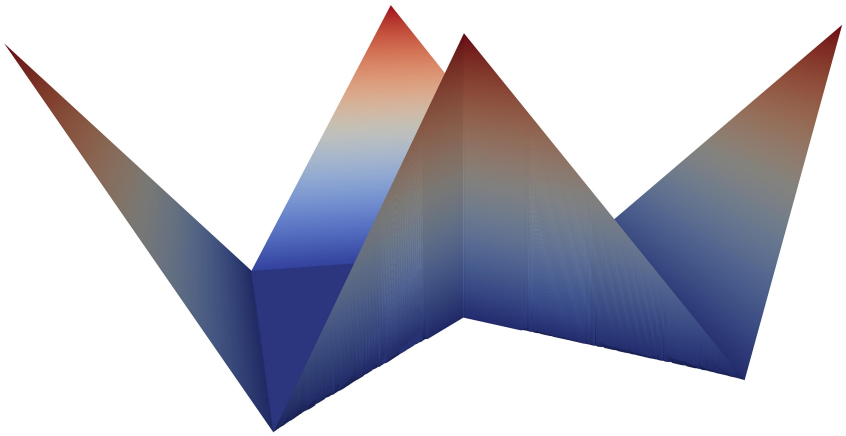

Figure 6. The figure shows a numerical solution of Experiment 5.2.

a non-convex domain.

Yet, also in this setting the numerical scheme of [6] is guaranteed to have a unique solution for any mesh. From our point of view this makes numerical experiments interesting.

Indeed, equations of Monge–Ampère type have been proposed for physical and biological models where the application does not justify to impose convexity on Ω or g. An example is the Monge–Ampère Keller–Segel system of chemotaxis [3, 11]. There the solution of a Monge–Ampère equation describes the density of a chemical substance, whose physical domain must not necessarily be convex.

Experiment 5.1 (Non-convex boundary data on the L-shape). Combining in spirit the domain of Experiment 3.2 with the boundary data of Experiment 4.1, we set $g(x) = x_2(1-x_2)$ on left boundary segment $\Gamma := \partial\Omega \cap \big[\{-1\} \times (0,1)\big]$ of the L-shape $\Omega = \big[(0,1)\times(-1,1)\big] \cup \big[(-1,1)\times(0,1)\big]$. On the remainder $\partial\Omega \setminus \Gamma$ we set $g(x) = x_1^4 - 1$ and on Ω we select $f = 0$.

Similarly to the previous experiment, numerical solutions approximate a multi-valued solution in the vicinity of Γ, while on the subdomain $\omega := \{x \in \Omega : x_1 > -0.95\}$ the numerical solutions converge under mesh refinement to $u(x) = x_1^4 - 1$. We see a relative $L^\infty(\omega)$ error of $4.8 \cdot 10^{-5}$ on a mesh with 168961 DoFs and $m = 64$, cf. Figure 5. Overall the largest number of Newton iterations in this computational experiment is 25, which occurs on the finest mesh with $m = 32$.

In the next experiment we consider a non-smooth solution of the degenerate equation (i.e. with $f = 0$), where the boundary data is non-convex and non-smooth at the re-entrant corner of the L-shape. Also in this more challenging setting the numerical method appears to be convergent, provided suitable scaling of m.

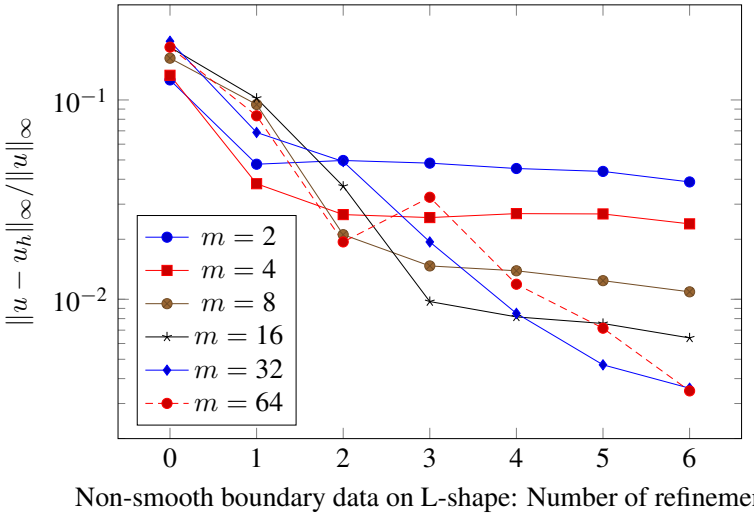

Figure 7. Relative $L^\infty(\omega)$-error for the test problem of Experiment 5.2.

Experiment 5.2 (Non-smooth non-convex boundary data at re-entrant corner). Let $g = \big||x_1|+|x_2|-1\big|$ be the boundary data on the L-shape Ω and $f = 0$. Our candidate solution u is equal to g on $\partial\Omega$ and equal to the convex envelope of g on Ω:

$$u:\ \overline{\Omega} \to \mathbb{R},\ x \mapsto \begin{cases} g & : \|x\|_1 \geq 0 \text{ or } x \in \partial\Omega, \\ 0 & : \|x\|_1 < 0 \text{ and } x \in \Omega. \end{cases}$$

The approximation u_h of u on a mesh with 466337 DoFs and $m = 64$ is shown in Figure 6. Measuring the error on the subdomain

$$\omega = \{(x_1, x_2) \in \Omega :\ x_1 \geq 0.1 \text{ or } x_2 \geq 0.1\},$$

a relative error $\|u-u_h\|_{L^\infty(\omega)}/\|u\|_{L^\infty(\omega)}$ of $3.47\,10^{-03}$ is observed for the numerical solution of that figure, while the corresponding relative error in the $L^2(\omega)$-norm is $2.03\,10^{-04}$. The full convergence graph of this experiment is shown in Figure 7, where the coarsest mesh has 137 DoFs and the finest 466337 DoFs.

The multi-valued behaviour may also be exhibited by problems with convex or even vanishing boundary data, when no smooth classical subsolution exists.

Experiment 5.3 (Hölder domain). We now consider the heart-shaped domain

$$\begin{aligned}\Omega = &\big[\big(B_{0.5}((0,0.5)) \cup B_{0.5}((0,-0.5))\big) \cap \{x \in \mathbf{R}^2 : x_1 \geq 0\}\big] \\ &\cup \big[B_1((0,0)) \cap \{x \in \mathbf{R}^2 : x_1 \leq 0\}\big],\end{aligned}$$

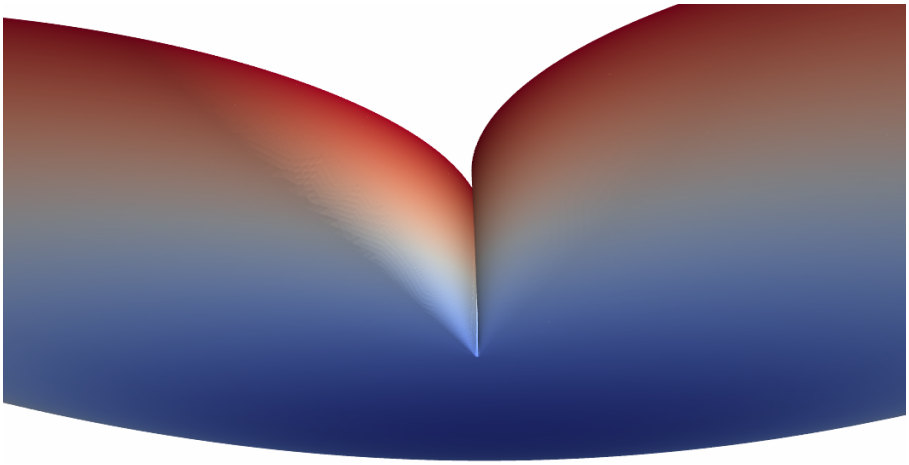

(a) Close-up view onto the numerical solution at non-convex part of Ω.

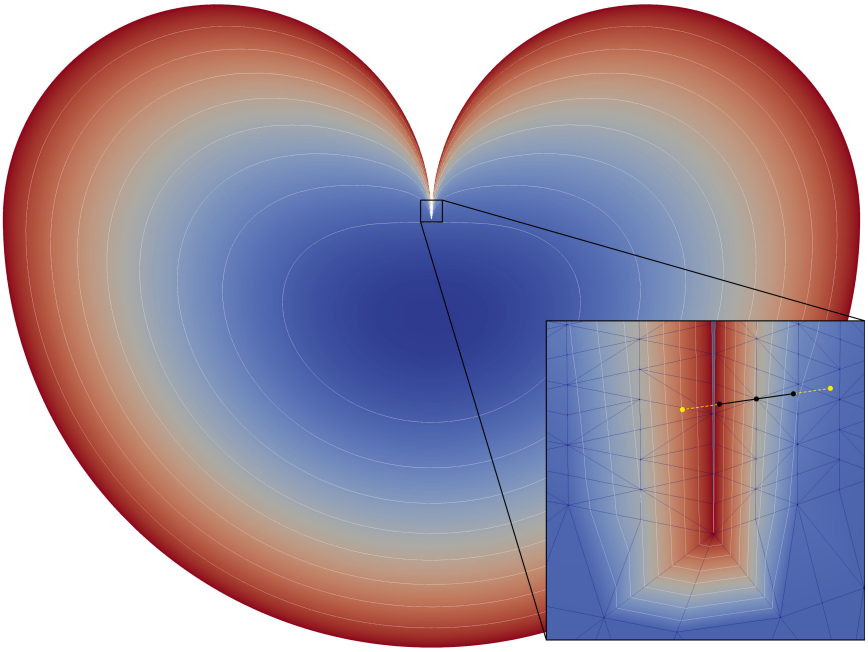

(b) Numerical solution with contour lines.

Figure 8. It appears that the numerical solution of Experiment 5.3 approximates the transition from a multi-valued boundary condition at the origin to a classical boundary condition on the remainder of the boundary; see the close-up (a) and also in the (b) the concentration of contour lines within the width of a single element at the origin. A cartoon stencil in (b) shows that careful scaling of the stencil is important to ensure that the finite differences approximate the local features of the solution.

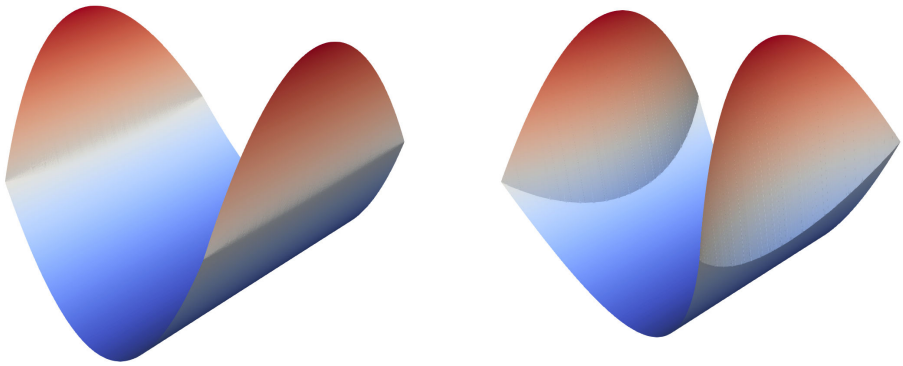

(a) (b)

Figure 9. The figure shows the numerical solutions in the two domains with $c = 3$ of Experiment 5.4, on the left with convex and on the right with concave faces.

where again $B_\delta(x)$ denotes the ball with radius δ and centre x. This domain does not satisfy a Lipschitz condition at the origin, as can also be seen in Figure 8 (b). In this example the boundary data $g = 0$ vanishes, while $f = 1$.

The plots of Figure 8 give the impression that at the origin the numerical solution approximates a multi-valued function but then transitions to a classical single-valued boundary condition. The stopping criterion for the Newton method is again a Newton step size of $5 \cdot 10^{-8}$, which is reached after 16 iterations in the computation with 166,176 DoFs and $m = 4$.

A note about the stencil diameter: As the cartoon stencil in Figure 8 (b) illustrates, a too simple implementation a wide second-order central difference with the centre on the right of the re-entrant boundary could have a node in Ω which is on the left of the re-entrant boundary. On non-convex domains stencils should be scaled so that not just the nodes of the stencil belong to Ω, but also any points between them.

Experiment 5.4 (Bent square). In this last experiment we solve the simple Monge–Ampère equation with $f = 0$ on a sequence of curved polyhedra, starting from a uniformly convex geometry and leading to polyhedra with concave faces:

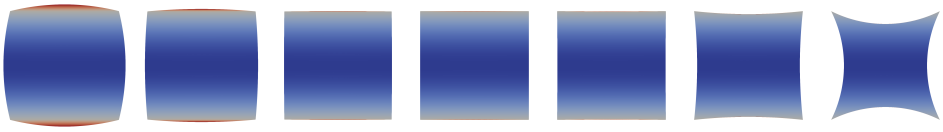

To be precise: The first three domains are formed from the intersection of four circles with the midpoints $(c, 0)$, $(0, c)$, $(-c, 0)$, $(0, -c)$ where c is 3, 10, 100 respectively

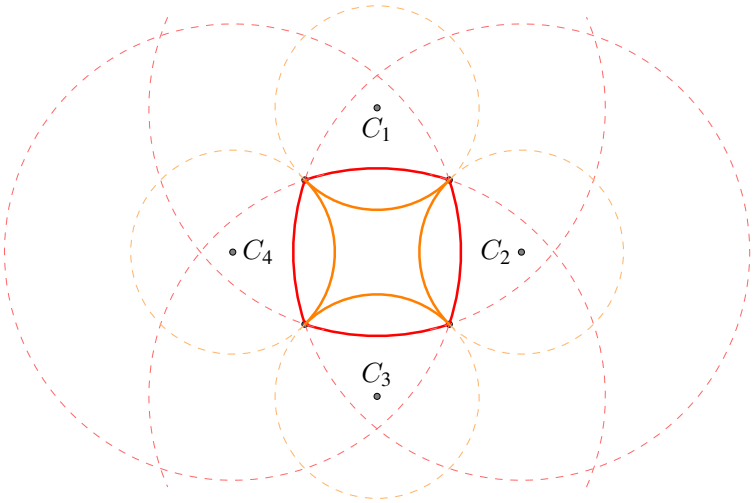

Figure 10. The 'bent square' domains are constructed from unions and intersections of circles about C_1, C_2, C_1 and C_4 with the square $[-1,1]^2$.

and where the radii are chosen so that the circles intersect at the points $(1,1)$, $(-1,1)$, $(1,-1)$ and $(-1,-1)$. The fourth domain is the square centred at the origin with side length 2. The remaining three domains are obtained by subtracting from this square the points which lie in circles with the same centres and intersection points as above, but smaller radii, see Figure 10.

With $f = 0$ the graphs of the exact solutions are (when restricted to the interior) surfaces of vanishing Gauss curvature. The function g is equal to the convex function $x_2^2 - 1$ where $|x_1| > |x_2|$ and equal to the concave function $1 - x_1^2$ where $|x_1| \leq |x_2|$. We note that g is continuous on $\partial\Omega$. Two of the resulting solutions are plotted in Figure 9. In the interior the numerical solutions do not significantly vary from the function $x_2^2 - 1$, which already defined the convex part of the boundary data. This is notable because on strictly convex domains the boundary function g is attained on all of $\partial\Omega$ in the classical single-valued sense, while on the other domains the multi-valued cut-off mechanisms appears to screen out concave sections of g. Indeed on $\omega = (-3/4, 3/4)^2$ we find the following relative L^∞ errors, taking $x_2^2 - 1$ as the reference solution:

domain	1	2	3	4	5	6	7
rel. $L^\infty(\omega)$-error	1.4e-3	1.3e-3	1.4e-3	1.4e-3	1.2e-3	1.2e-3	8.7e-4
# Newton	10	10	9	9	14	20	20

The table also shows an increase in the required Newton iterations to achieve a Newton step size of $5 \cdot 10^{-8}$ when the faces of Ω are concave. The number of DoFs vary in this experiment between 108,124 and 140,324, depending on the domain.

6 Conclusions

In conclusion, we addressed the aims set out in the introduction. After the reformulation as a Bellman operator the numerical solution of the Monge-Ampère equation does not appear to be significantly more difficult if convexity of the domain and boundary data are dropped. As long as $h/m \to 0$ and $m \to \infty$ under h-refinement as in [6] the numerical solutions appear to converge to a unique limit, also in case of non-Lipschitzian or non-simply connected Ω or when a loss of pointwise boundary conditions occurs. The numerical experiments are presented for domains in $\mathbf{R}^2$; however, we have no reason to suspect a fundamentally different behaviour in higher dimensions.

Bibliography

[1] I.J. Bakelman. *Generalized elliptic solutions of the Dirichlet problem for n-dimensional Monge-Ampère equations. Proc. of Symposia in Pure Math.*, 45:73–102, 1986.

[2] G. Barles, P.E. Souganidis. *Convergence of approximation schemes for fully nonlinear second order equations. Asymptotic Anal.*, 4(3):271–283, 1991.

[3] Y. Brenier. *Optimal transport, convection, magnetic relaxation and generalized Boussinesq equations. Journal of Nonlinear Science.*, 19(5):547–570, 2009.

[4] M.G. Crandall, H. Ishii, P.-L. Lions. *User's guide to viscosity solutions of second order partial differential equations. Bull. Amer. Math. Soc.*, 27(1):1–67, 1992.

[5] G. De Philippis, A. Figalli. *Optimal regularity of the convex envelope. Trans. Amer. Math. Soc.* 367:4407–4422, 2015.

[6] X. Feng, M. Jensen. *Convergent semi-Lagrangian methods for the Monge-Ampère equation on unstructured grids.* SIAM J. Numer. Anal. 55:691–712, 2017.

[7] B. Guan, J. Spruck. *Boundary-value problems on S^n for surfaces of constant Gauss curvature. Annals of Mathematics.* 138:601–624, 1993.

[8] B. Guan. *The Dirichlet problem for Monge-Ampère equations in non-convex domains and spacelike hypersurfaces of constant Gauss curvature. Trans. Amer. Math. Soc.* 350:4955–4971, 1998.

[9] C.E. Gutiérrez. *The Monge-Ampère equation.* Birkhäuser, 2001.

[10] B. Froese Hamfeldt *Convergent approximation of non-continuous surfaces of prescribed Gaussian curvature.* Communications on Pure and Applied Analysis 17:671-707, 2018.

[11] H. Huang, J.-G. Liu. *A note on Monge–Ampère Keller–Segel equation.* Applied Mathematics Letters, 61:26–34, 2016.

[12] M. Jensen, I. Smears. *On the notion of boundary conditions in comparison principles for viscosity solutions.* arXiv 1703.07313, 2017.

[13] N.V. Krylov. *Nonlinear elliptic and parabolic equations of the second order.* Springer, 1987.

[14] N.V. Krylov. *Interior estimates for second-order differences of solutions of finite-difference elliptic Bellman's equations. Math. Comp.* 82:1463-1487, 2013.

[15] T.S. Motzkin, W. Wasow *On the approximation of linear elliptic differential equations by difference equations with positive coefficients. Journal of Math. Physics*, 31:253–259, 1953.

Author information

Max Jensen, Department of Mathematics, University of Sussex, Brighton BN1 9QF, England.
E-mail: m.jensen@sussex.ac.uk